Journal of Applied Electrochemistry **30**: 77–83, 2000.

Changes in positive lead/acid battery plates during charge/discharge cycling

R. DE MARCO* and J. JONES
School of Applied Chemistry, Curtin University of Technology, GPO Box U 1987, Perth, Western Australia, 6845, Australia
*(*author for correspondence)*

Received 8 March 1999; accepted in revised form 25 June 1999

Key words: grid corrosion layer, lead/acid battery, plate passivation, positive active material, premature capacity loss

Abstract

Active materials and corrosion layers in positive plates of nonantimonial lead/acid batteries, at different stages of charge/discharge cycling, have been characterized by using scanning electron microscopy (SEM), X-ray diffraction (XRD) and X-ray photoelectron spectroscopy (XPS). In the initial stages of cycling, it has been found that the observed overcharging of cells is responsible for the formation of an underlayer of PbO in the grid corrosion layer, and this blocks the transfer of charge to the current collecting grid, causing rapid capacity loss. In the later stages of cycling at a ratio of capacities for charge and discharge (i.e., C/D) of close to unity, the grid corrosion layer does not possess an underlayer of PbO; however, the active material becomes progressively enriched with respect to insulating lead sulfate. It is suggested that initial overcharging is symbolic of grid corrosion as the rate of gassing side reactions is kept to a minimum by restricting the top-of-charge-voltage (TOCV) to 2.55 V, while sulfation of active material occurring at C/D values of about unity is probably attributable to stratification of the electrolyte and its concomitant effect on sulfation of active material.

1. Introduction

Premature capacity loss (PCL) causes the early failure of lead/acid acid batteries in deep discharge applications [1]. The phenomenon of PCL originates through passivation of positive plates within the grid corrosion layer and/or active material [2, 3]. Numerous authors [4–9] have demonstrated that a significant factor in PCL is a diminution in the conductivity of positive active material (PAM) as a result of either sulfation [4–6] and/or disintegration of the interparticle network of PAM that is responsible for electrical connection of zones within the active mass [7–9].

At present, the preferred explanation for PCL [10] is a diminution in the aggregation of spheres within the PAM along with its concomitant effect on battery life. Some authors [1, 9] claim that passivation of the grid corrosion layer plays a minor role in PCL. The present authors' suggest that it is not possible to ignore the role of grid corrosion as there is ample evidence demonstrating the deleterious effects of this important phenomenon [2, 3, 8, 11, 12].

A recent study [13] has revealed that deliberately invoked hydrocerussite (a basic lead carbonate) on nonantimonial grids had a detrimental effect on the charge/discharge cycling behaviour of lead/acid batteries. It is very likely that this phenomenon is a manifestation of the grid corrosion pattern occurring beneath the layer of basic lead carbonate. A second important feature of this recent work [13] was the suggestion that grid corrosion, as proposed elsewhere by other authors [2, 3, 8, 11], predominates in the initial stages of cycling at a ratio of capacities for charge and discharge (i.e., C/D) of greater than unity, while sulfation of PAM [5, 6, 14–16] is probably a significant factor contributing to battery failure towards the end of cycling as C/D approaches unity.

Although the preferred explanation for PCL relates to the aggregate-of-spheres model for PAM [10], it appears that the influence of passivation of the grid corrosion layer and sulfation of the PAM cannot be disregarded. The aim of this study has been to undertake characterization of positive plates at various stages of cycling to ascertain the relative importance of different forms of plate passivation (grid corrosion layer, active material network and/or sulfation of PAM). PAM and grid corrosion layers have been studied using scanning electron microscopy (SEM), X-ray diffraction (XRD) and X-ray photoelectron spectroscopy (XPS).

2. Experimental details

2.1. *Assembly and charge/discharge cycling of 2 V cells*

Positive plates were prepared using the paste formula and procedures that have been described elsewhere [13]. The paste was applied by hand to lead-calcium-tin grids that are commonly used in the manufacture of GNB Powersafe batteries. Analysis of the grids using inductively-coupled plasma atomic emission spectrometric analysis revealed that they contained 0.1 wt % Ca and 0.4 wt % Sn [17]. The plates were then cured at 50 °C and high humidity for two days.

The pasted and cured plates were assembled into 2 V cells, comprising one positive plate surrounded by two factory manufactured negative plates, using the procedures described elsewhere [13]. The plates were formed in 1.2 dm^3 of 1.07 relative density H_2SO_4 using a constant current of 5 A for 6 h, and then rested at open circuit for 1 h to allow the sulfuric acid depleted diffusion layers of the pores to be replenished by the permeation of fresh electrolyte. The charge/rest period was repeated, followed by a final constant current charge of 5 A for 6 h. After formation, the sulfuric acid and separators were discarded, and the cells were reassembled and filled with 1.3 dm^3 of 1.270 relative density H_2SO_4.

The cycle-life performance of 2 V cells was assessed by employing a Digatron BTS-500 computerized charge/discharge unit (Digatron GmbH, Germany) to undertake repetitive charge/discharge cycling at the 3 h rate. After charging to 2.55 V at a constant current of 5.6 A, the cells were held at the top-of-charge voltage (TOCV) until the current had tapered to 1 A. At this juncture, the cells were discharged at a constant current of 5.6 A until the voltage dropped to 1.75. The charge/discharge procedure was repeated until the discharge capacity fell to 50% of its original value.

2.2. *Analyses of cells*

At the end of cycling, the cells were returned to the fully charged state by charging them at a constant current of 4 A up to a TOCV of 2.55 V, and holding them at this voltage until the current had fallen to 1 A. The charged cells were dismantled, and the positive plates were rinsed in distilled water followed by drying at 50 °C for 24 h. The wet positive plates and glass separators were inspected manually to ascertain if active material shedding was a significant cause of cell failure. The PAM of dry positive plates was analysed by XRD using a Kristalloflex Siemens D500 X-ray diffractometer fitted with a CuK_α X-ray tube that was operated at an accelerating voltage of 20 kV and a beam current of 30 mA.

The grid corrosion layers of epoxy-mounted, polished cross sections of positive plates were examined by SEM using a Phillips XL30 electron microscope operated at an accelerating voltage of 25 kV, and a spot size setting of 4. The specimens were ground successively on 500, 1000 and 1200 grit emery paper using a paraffin lubricant and a Struers Dap-V disc polisher that was rotated at 300 rpm. After grinding, the specimens were polished successively on Struers DP-Spray, P diamond sprays (3 and 1 μm) that had been applied to DP-Nap and DP-Mol felt pad discs using a rotation speed of 300 rpm and the Struers DP-lubricant Red.

XPS was carried out on a VG Escalab 220 IXL at the University of New South Wales using AlK_α X rays. Small sections of epoxy-mounted cross sections were prepared by using the same procedure employed in the SEM analysis of grid corrosion layers. The specimens were cleaned prior to XPS analysis by subjecting them to 5 min of argon ion etching.

3. Results and discussion

3.1. *Cycling behaviour of cells*

In a previous study [13], two distinct regions of PCL were identified for nonantimonial 2 V cells that had been subjected to a self-regulated charge/discharge cycling regime (viz., charging at a constant current of 5.6 A up to a TOCV of 2.55 V, at which point the current is allowed to taper to 1 A, before switching to discharge at a constant current of 5.6 A until the terminal voltage falls to 1.75 V). It was found that rapid capacity loss, designated by a 30% drop in the discharge capacity compared to the initial value, occurred between 1 and 10 cycles, while a diminished rate of capacity loss, signified by a further 10% fall in discharge capacity compared to the initial value, prevailed between 10 and 30 cycles. Significantly, it was also found that this disparate behaviour in PCL was linked to C/D values at different stages of cycling (viz., rapid capacity loss corresponded to $C/D > 1$, while slow capacity loss was associated with $C/D \approx 1$).

As the lead/acid battery is a reversible electrochemical system, it has been hypothesized [13] that rapid grid corrosion caused by cell overcharging, as proposed elsewhere by other authors [2, 3, 8, 11], produces a passivation layer at the active material/grid corrosion layer interface (probably α-PbO), and this reduces both the exchange of electrons and the capacity during the discharge step of the cycle. Significantly, it was shown that water decomposition side reactions were minimal during cycling, and the cells did not lose any water throughout testing.

In [13] it was also suggested that growth of the corrosion layer involves the conversion of outer PbO to PbO_2 while additional PbO forms at the grid/corrosion layer interface as the grid continues to corrode. This scenario is consistent with other reports [3] of a bilayer corrosion film on non-antimonial grids. In such a case, grid corrosion will be minimal under conditions of little or no overcharging (i.e., $C/D \approx 1$) in the later stages of

cycling (i.e., 10–30 cycles), and sulfation of PAM [5, 6, 14–16] along with diminution in the aggregation of spheres within the PAM [7–9, 18–20] are expected to cause PCL under these conditions.

The present work involves a characterization of the corrosion layers and active materials of positive plates in different regions of PCL to ascertain the exact cause of the two types of PCL behaviour.

3.2. *Characterization of positive plates at different stages of cycling*

3.2.1. *SEM studies of corrosion layers*

Figure 1(a) and (b) present SEM backscattered electron micrographs for polished, epoxy-mounted cross sections of positive plates that have been subjected to 6 and 12 cycles, respectively. It is evident that the corrosion layer of the positive plate after six cycles is made up of two compositionally different films (viz., possibly an underlayer of PbO, and an overlayer of PbO_2). This observation is internally consistent with the electron probe microanalysis data in [3], which also suggested a bilayer corrosion film of PbO and PbO_2 on nonantimonial battery plates. By contrast, the plate subjected to 12 cycles yielded a uniform corrosion layer that is probably composed of PbO_2.

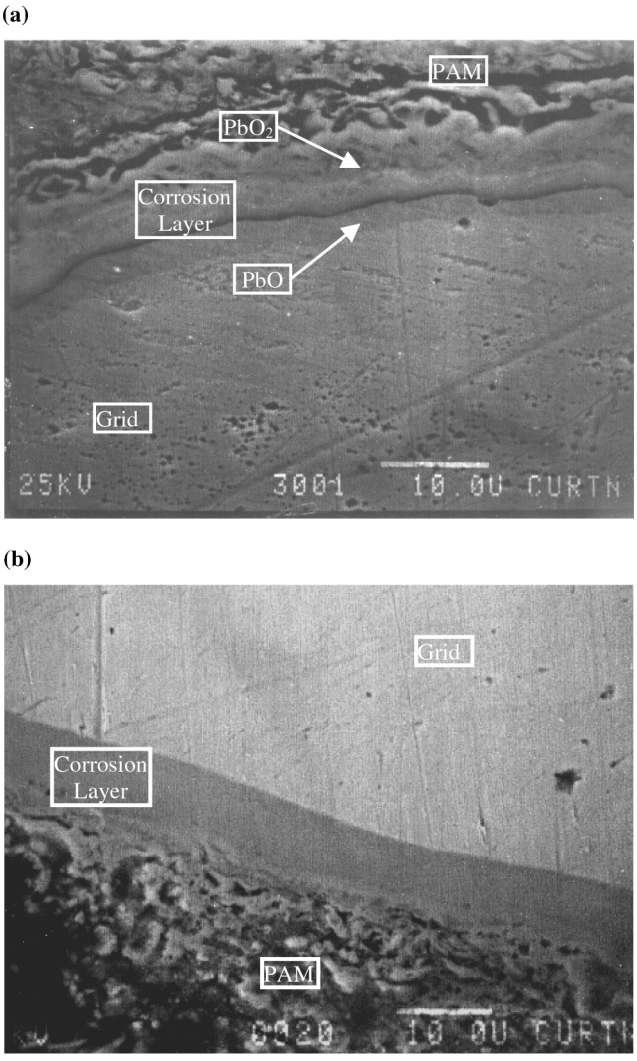

Fig. 1. Backscattered SEM micrographs of polished, epoxy-mounted cross sections of positive lead/acid battery plates at (a) 6 and (b) 12 cycles. Scalebar 10 μm.

In summary, the SEM results imply that an insulating underlayer of PbO is formed in the corrosion layer of nonantimonial lead/acid battery plates in the initial stages of cycling when cell overcharging occurs (viz., $C/D > 1$). In contrast, the corrosion layer ceases to grow in the later stages of cycling at C/D values of close to unity, and the underlayer film of PbO is probably oxidised to PbO_2.

3.2.2. *XPS studies of corrosion layers*

The chemical species in the bilayer corrosion film of cycled positive lead/acid battery plates have been identified using selected area XPS. XPS line scans for Pb, PbO and PbO_2 (through small sections of polished, epoxy-mounted cross-sections of plates) have been used in the characterization of corrosion layers. It is important to note that the spatial resolution of the XPS line scans is 2 μm.

Figure 2 presents the XPS spectrum of the Pb($4f_{7/2}$) level for an analysis region comprising both the corrosion layer and the lead grid of a positive plate that had been subjected to 6 cycles. The presence of two partially resolved peaks is indicative of at least two Pb species; however, the broadness of the high binding energy shoulder at 138 eV implies that this shoulder is made up of more than one Pb species. Curve fitting of three peaks with full width at half maxima (FWHM) of 0.9 eV yielded a very good fit to the experimental data (refer to the upper two lines in Figure 2). The three peaks at 136.5, 137.7 and 138.3 eV are representative of Pb, PbO_2 and PbO, respectively [21].

The Pb, PbO and PbO_2 Pb($4f_{7/2}$) XPS line scans for a positive plate subjected to six cycles are presented in Figure 3(a), (b) and (c), respectively. Images of the sample revealed that the lack of Pb signals from 100–130 μm is due to the epoxy mounting of the cross section, while the Pb signals from 130–160 μm are attributable to PAM. Similarly, the Pb signals between 160–180 and 180–200 μm are attributable to the grid corrosion layer and lead grid, respectively. As expected, the XPS results demonstrate that the PAM (i.e., 130–160 μm) is rich in PbO_2, while the corrosion layer in contact with the grid (i.e., 170–180 μm) is enriched with respect to PbO and deficient in PbO_2. Significantly, the PAM also reveals low amounts of PbO (see Figure 3(b)), and this is probably due to the formation of a non-stoichiometric PbO_{2-x} phase involving Pb^{2+} doping of the PbO_2 lattice [2].

By comparison, the Pb($4f_{7/2}$) line scans for the positive plate subjected to 12 cycles (refer to Figure 4) show a 20 μm corrosion layer that is intimately contacting the grid between 140–160 μm, with the trend for PbO signals mirroring that for PbO_2 signals. This

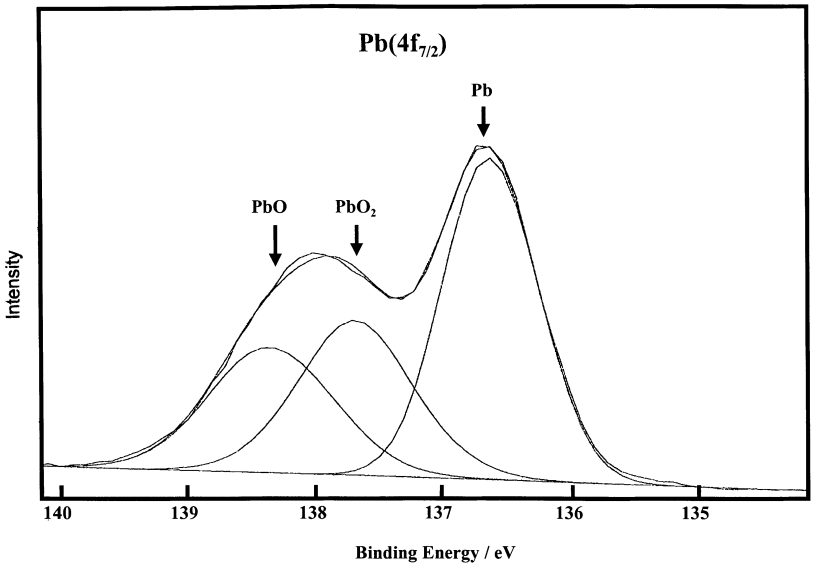

Fig. 2. XPS spectrum of the $Pb(4f_{7/2})$ level for an analysis region encompassing both the corrosion layer and the lead grid of a lead/acid battery plate that had been subjected to six cycles.

observation is inconsistent with the presence of any PbO rich regions in the grid corrosion layer (i.e., between 140 and 160 μm), suggesting the formation of a uniform PbO_{2-x} corrosion layer comprising a Pb^{2+} doped PbO_2 metal sublattice [2]. It is important to note that the PAM had broken away from the grid during the preparation of this epoxy-mounted cross section.

In summary, the selected area XPS results confirm that PbO forms in the underlayer of the corrosion film of nonantimonial plates during the initial stages of cycling at high C/D values; however, a uniform layer of PbO_{2-x} is formed in the later stages of cycling whereby the cessation of grid corrosion occurring at C/D values of about unity enables the oxidation of PbO to PbO_{2-x}.

3.2.3. *XRD phase composition of PAM*

Samples of PAM at different stages of cycling were taken from a central vertical transect through the plates, removing material at the top, centre and bottom of the plates. This sampling scheme was employed as a means of examining the sulfation of active material accompanying stratification of the sulfuric acid electrolyte [5, 6, 14–16].

The $PbSO_4$ XRD line intensities have been normalised with respect to the integrated intensities for $PbSO_4$, α-PbO_2 and β-PbO_2, using 100% peaks, and the results are presented in Table 1. As cycling proceeds, it can be seen that the $PbSO_4$ content of PAM increases in the centre and bottom sections of the cycled plates. Other authors [6] have measured the variation in relative density of sulfuric acid as a function of depth and cycling, along with the XRD phase compositions of PAM at different plate locations' noting it was shown that high concentrations of $PbSO_4$ are found at the base of positive plates that have been exposed to elevated levels of sulfuric acid that arise from stratification of the electrolyte. The authors' present XRD data at the end of cycling for C/D values approaching unity strongly suggest that stratification of the electrolyte is responsible for the sulfation of plates under these conditions. Note that it was not possible to measure the relative densities of electrolyte as a function of depth and cycling in the present study because absorptive glass mat separators were used; however, the open circuit voltage (OCV) of the fully charged cells diminished as cycling proceeded, and it has been proposed elsewhere [14] that a drop in OCV is a good indicator of stratification of the electrolyte and sulfation of the PAM. As proposed elsewhere by other authors [4, 5], it is likely that stratification of the electrolyte occurs at $C/D \approx 1$ as there is little or no agitation of the electrolyte by gassing side reactions at low values of TOCV. It is also possible that the high levels of sulfuric acid at the bottom of cycled cells is likely to cause a preferential discharge of the PAM in this region, causing a localized degradation in the aggregation of particles in the PAM, and localized PCL [16]. The authors believe that PCL in the later stages of cycling is attributable to a combination of these phenomena.

4. Conclusion

The results of this study demonstrate the power of selected area XPS for investigating the corrosion layers of lead/acid battery plates. It has been shown unequivocally that the bilayer corrosion film of nonantimonial battery plates comprises an overlayer of PbO_2, and an underlayer of PbO. The presence of an insulating layer of PbO affects deleteriously the charge/discharge cycling behaviour of positive lead/acid battery plates.

Although it is generally acknowledged that the major cause of PCL in lead/acid batteries is attributable to a

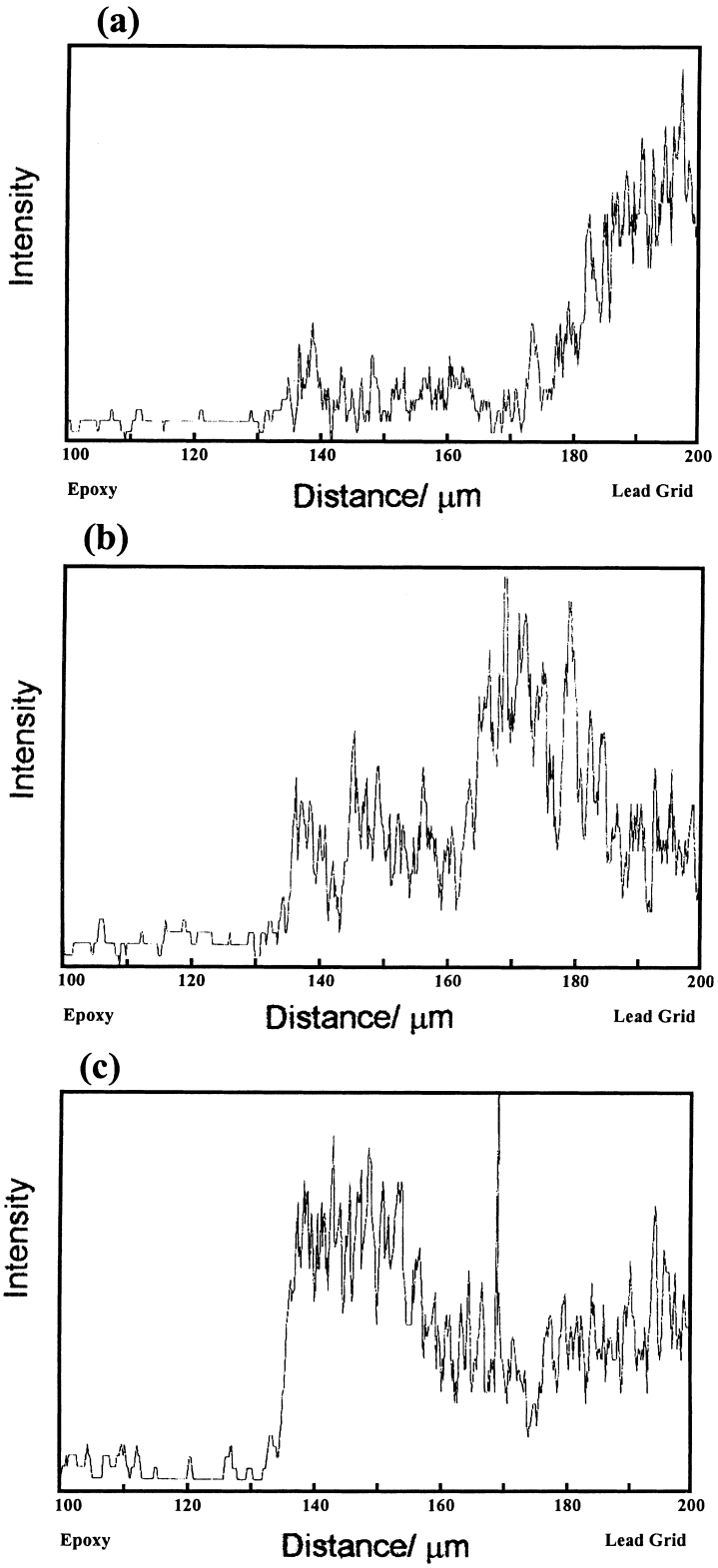

Fig. 3. XPS line scans for a polished, epoxy-mounted cross section of a positive lead/acid battery plate that has been subjected to six cycles: (a) Pb; (b) PbO; (c) PbO_2.

diminution in the aggregate-of-spheres within the PAM, the link between the formation of insulating PbO at high values of C/D, as noted in this study, demonstrates that grid corrosion is another important contributor to PCL under these conditions.

In the later stages of cycling at C/D values approaching unity, it is evident that growth of the corrosion layer ceases and the underlayer of PbO is oxidised to PbO_2, generating a uniform corrosion layer. XRD phase composition data for PAM have demonstrated that

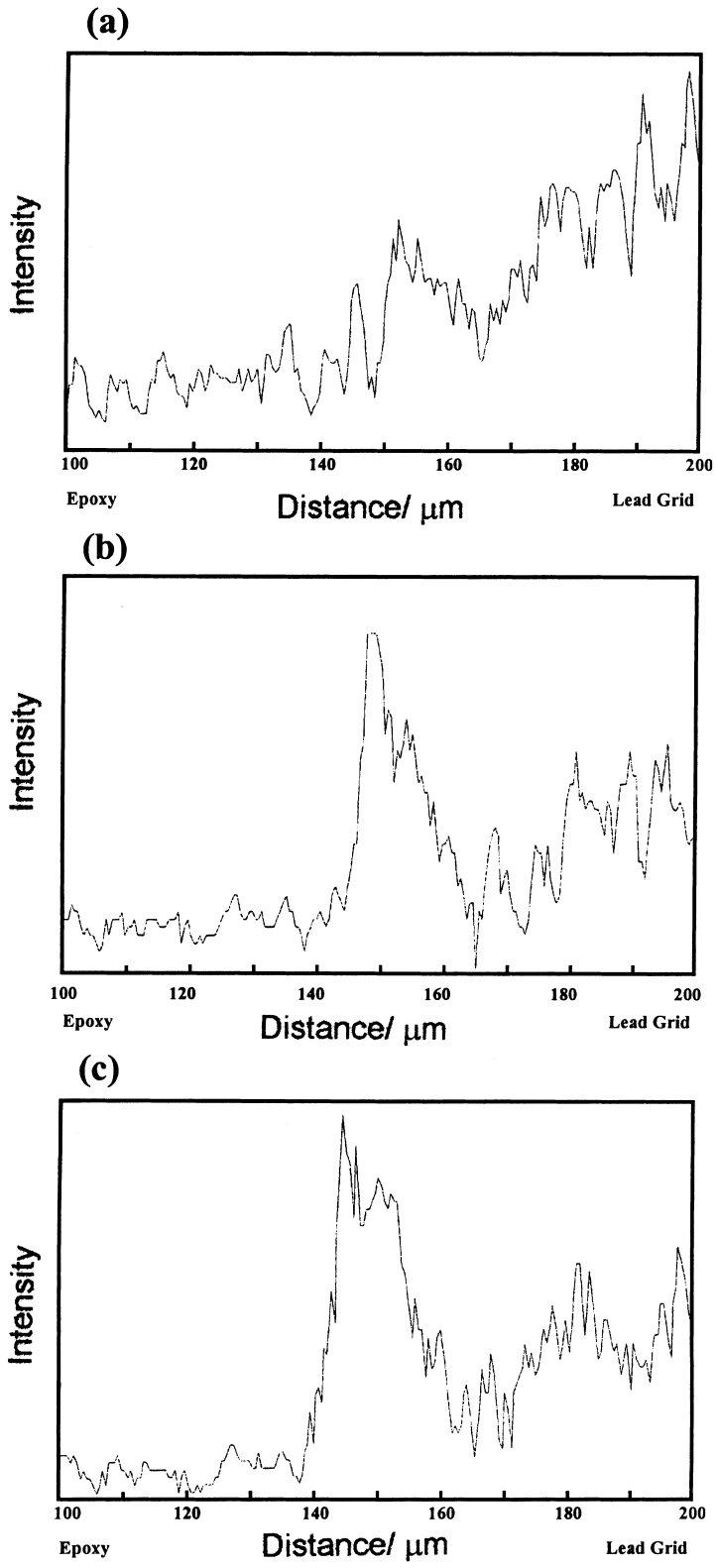

Fig. 4. XPS line scans for a polished, epoxy-mounted cross section of a positive lead/acid battery plate that has been subjected to 12 cycles: (a) Pb; (b) PbO; (c) PbO_2.

the slow discharge capacity loss occurring in the later stages of cycling is attributable partly at least to stratification of the electrolyte, and sulfation of the active material.

Acknowledgements

The authors thank GNB Battery Technologies for providing the battery materials used in this study, along

Table 1. Lead sulfate XRD diffraction line intensities normalized to the integrated intensity of all detected phases (i.e., α-PbO_2, β-PbO_2 and $PbSO_4$)

Cycle	Intensity ($PbSO_4$)/%		
	Top	Centre	Bottom
3rd	0.43	1.3	2.1
6th	0.52	1.7	8.9
9th	1.2	3.0	24.1
12th	1.5	7.7	17.8
15th	1.1	10.4	25.2
18th	1.2	11.2	24.3

with the Australian Research Council and Alternative Energy Development Board for financial assistance. We thank Dr Leong Mar and Assoc. Prof. R. Lamb of the University of New South Wales for undertaking the selected area XPS analyses.

References

1. K.K. Constanti, A.F. Hollenkamp, M.J. Koop and K. McGregor, *J. Power Sources* **55** (1995) 269.
2. D. Pavlov, *J. Power Sources* **53** (1995) 9.
3. A.F. Hollenkamp, K.K. Constanti, M.J. Koop, L. Apateanu, M. Calabek and K. Micka, *J. Power Sources* **48** (1994) 195.
4. H. Dietz, H. Niepraschk, K. Wiesener, J. Garche and J. Bauer, *J. Power Sources* **46** (1993) 191.
5. L. Apateanu, A.F. Hollenkamp and M.J. Koop, *J. Power Sources* **46** (1993) 239.
6. C.W. Chao, S.P. Lin, Y.Y. Wang, C.C. Wan and J.T. Yang, *J. Power Sources* **55** (1995) 243.
7. A. Winsel, E. Voss and U. Hullmeine, *J. Power Sources* **30** (1990) 209.
8. D. Pavlov, *J. Power Sources* **48** (1994) 179.
9. M. Calabek, K. Micka, P. Baca, P. Krivak and V. Smarda, *J. Power Sources* **62** (1996) 161.
10. P.T. Moseley, *J. Power Sources* **59** (1996) 81.
11. D. Pavlov, A. Dakhouche and T. Rogachev, *J. Appl. Electrochem.* **27** (1997) 720.
12. A. El Ghachcham Amrani, Ph. Steyer, J. Steinmetz, P. Delcroix and G. Le Caer, *J. Power Sources* **64** (1997) 35.
13. R. De Marco, *J. Appl. Electrochem.* **27** (1997) 99.
14. R. Wagner, *J. Power Sources* **53** (1995) 153.
15. D.U. Sauer, *J. Power Sources* **64** (1997) 181.
16. R.H. Newnham and W.G.A. Baldsing, *J. Power Sources* **66** (1997) 27.
17. R. De Marco and J. Liesegang, *Appl. Surf. Sci.* **84** (1995) 237.
18. E. Bashtavelova and A. Winsel, *J. Power Sources* **67** (1997) 93.
19. S. Atlung and T. Jacobsen, *J. Power Sources* **66** (1997) 147.
20. A.F. Hollenkamp, *J. Power Sources* **59** (1996) 87.
21. J.F. Moulder, W.F. Stickle, P.E. Sobol and K.D. Bombden (Eds), 'Handbook of X-ray Photoelectron Spectroscopy' (Perkin-Elmer, Eden Prairie, MN, 1992).